Influence of Pearlite Morphology and Heating Rate on the Kinetics of Continuously Heated Austenite Formation in a Eutectoid Steel

F.G. CABALLERO, C. CAPDEVILA AND C. GARCÍA DE ANDRÉS

ABSTRACT

A model that describes pearlite-to-austenite transformation during continuous heating in a eutectoid steel has been developed. The influence of structure parameters, such as interlamellar spacing and edge length of pearlite colonies, and heating rate on the austenite formation kinetics has been experimentally studied and considered in the modeling. It has been found that the kinetics of austenite formation is slower the coarser the initial pearlite microstructure and the higher the heating rate. Moreover, both start and finish temperatures of the transformation slightly increase as heating rate does, but finish temperatures are more sensitive to that parameter. A good agreement (accuracy higher than 90% in square correlation factor) between experimental and predicted values has been found.

F.G. CABALLERO, Post-doctoral Research Assistant, and C. GARCÍA DE ANDRÉS, Senior Research Scientist, are with the Department of Physical Metallurgy, Centro Nacional de Investigaciones Metalúrgicas (CENIM), CSIC, Avda. Gregorio del Amo, 8, 28040 Madrid, Spain. C. CAPDEVILA, Post-doctoral Research Assistant, with the Department of Materials Science and Metallurgy, University of Cambridge, Pembroke Street, Cambridge CB2 3QZ, UK

I. INTRODUCTION

MOST commercial processes rely to some extent on heat treatments, which cause the steel to revert to the austenitic condition. This includes the processes involved in the manufacture of wrought steels and in the fabrication of steel components by welding. It is useful, therefore, to be able to model quantitatively the transformation of an ambient temperature steel microstructure into austenite[1].

The microstructure from which austenite may form can be infinitely varied (ferrite, martensite, carbide and various morphologies and aggregates of each, e.g. pearlite, bainite). Many variables are therefore needed to describe the kinetics of austenite formation. Factors such as particle size, the distribution and chemistry of individual phases, homogeneity, the presence of non-metallic inclusions, should all be important.[2-5] Thus, in the case of formation of austenite from pearlite one of the most relevant structural factor to be considered is the interlamellar spacing of pearlite.[6]

In fully pearlitic steel, austenite nucleates heterogeneously at the junctions between pearlite colonies. This is in spite of the relatively large amount of interlamellar surfaces available within the pearlite colonies, which seem to be much less effective as sites for the nucleation of austenite.[7] The rate of growth of the austenite is controlled primarily by the rate of carbon diffusion in the austenite between adjacent pearlitic cementite lamellae, but may also be influenced by boundary diffusion of substitutional alloying elements at low temperature.[3]

Models of specific metallurgical approaches exist for isothermal austenite formation from different initial microstructures.[3,7-13] However, none of these is likely to be of general applicability, except perhaps at slow heating rates consistent with the achievement of equilibrium. In this work a model is presented for the austenite formation during continuous

heating in a eutectoid steel with a fully pearlitic initial microstructure. The influence of the parameters such as interlamellar spacing of pearlite, edge length of pearlite colonies and heating rate on transformation kinetics has been considered in the model. Results of modeling have been experimentally validated at three different heating rates and for three different morphologies of pearlite.

TABLE I. Isothermal Conditions Employed for the Formation of Pearlitic Microstructures

Specimen	Temperature (K)	Time (min)
M1	948	45
M2	923	10
M3	798	60

II. EXPERIMENTAL PROCEDURE

A. Morphological characterization of lamellar pearlite

A eutectoid carbon steel with an actual composition (wt. %) of 0.76C, 0.24Si, 0.91Mn and 0.013P was used. Alloy was prepared as a 2500 kg vacuum induction melt from high purity base material. After casting and cropping, the ingot was hot rolled down to a 50 mm square bar. The following heat treatments were carried out to yield in this steel fully pearlitic microstructures with different scale parameters. Cylindrical samples of 2 mm in diameter and 12 mm in length were austenitized under vacuum (1 Pa) in a radiation furnace for 5 min at

1273 K, isothermally transformed at one of three different temperatures and subsequently cooled rapidly to room temperature. Table I lists all the temperatures and holding times used for the isothermal formation of pearlite with different morphological parameters in this steel.

Specimens were ground and polished using standardized techniques and finished on 0.25 μm diamond paste for metallographic examination. 2pct-Nital etching solution was used to reveal the microstructure by optical microscopy. Micrographs in Figure 1 confirm that 100 % transformation to pearlite occurs at all the heat treatments performed. An etching solution of picric acid in isopropyl alcohol with several drops of Vilella's reagent was also used to reveal pearlite in specimens M1 and M2 on a JEOL JXA-820 scanning electron microscope (SEM) (Figures 2.a and b). Pearlite in specimen M3 was characterized by transmission electron microscopy (TEM). For this, 3 mm diameter cylindrical samples were sliced into 100 μm thick discs and subsequently ground down to foils of 50 μm thickness on wet 800 grit silicon carbide paper. These foils were finally electropolished at room temperature until perforation occurred, using a twin-jet electropolisher set (E. A. Fischione Inst. Mfg – Model 110) at a voltage of 100 V. The electrolyte consisted of 5 % perchloric acid, 15 % glycerol and 80 % methanol. The foils were examined in a JEOL JEM-200 CX transmission electron microscope at an operating voltage of 200 kV. (Figure 2.c).

Two parameters, the mean true interlamellar spacing (σ_o) and the area per unit volume of the pearlite colonies interface (S_v^{PP}), are used to fully characterize the obtained lamellar microstructures.[8] The values of σ_o were derived from electron micrographs according to Underwood's intersection procedure. Underwood[14] recommends determining the mean random spacing σ_r first to estimate the mean true spacing σ_o. For this purpose, a circular test grid of diameter d_c is superimposed on an electron micrograph. The number n of intersections of lamellae of carbide with the test grid is counted. This procedure is repeated on at least fifty fields chosen randomly. Then, the mean random spacing σ_r is calculated from:

$$\sigma_r = \frac{\pi d_c}{nM} \qquad [1]$$

where M is the magnification of the micrograph.

Saltykov[15] has shown that, for pearlite with a constant spacing within each colony, the mean true spacing σ_o is related to the mean random spacing σ_r by:

$$\sigma_o = \frac{\sigma_r}{2} \qquad [2]$$

A pearlite nodule is composed of multiple colonies; each colony has parallel lamellae, which are orientated differently with respect to lamellae in adjacent colonies as Figure 3.a illustrates. The values of S_v^{PP} were derived from scanning electron micrographs at low magnification (Figure 3.b) by counting the number of intersections (n') of the pearlite colony boundaries with a circular test grid of diameter d'_c as reported by Roosz et al.[8] This procedure is repeated on at least fifty fields chosen randomly. Then, the area per unit volume of the pearlite colonies interface is:

$$S_v^{PP} = \frac{2n'M}{\pi d'_c} \qquad [3]$$

where M is the magnification of the micrograph.

Approximating the pearlite colony by a truncated octahedron (Figure 4) the edge length of the pearlite colonies (a^P) is calculated from the area per unit volume S_v^{PP} with the following expression[16]:

$$S_v^{PP} = \frac{6\left(1+2\sqrt{3}\right)\ (a^P)^2}{8\sqrt{2}\,(a^P)^3} = \frac{3\left(1+2\sqrt{3}\right)}{4\sqrt{2}\,a^P} \qquad [4]$$

Data for σ_o, S_v^{PP} and a^P are listed in Table II.

TABLE II. Morphological Characterization of Pearlite

Specimen	σ_o (μm)	$S_v^{PP}\times10^{-3}$ (μm^{-1})	a^P (μm)
M1	0.20±0.03	581±86	4.16±0.70
M2	0.08±0.01	1399±273	1.76±0.34
M3	0.06±0.01	1432±60	1.65±0.07

B. Dilatometric and metallographic analysis of austenite formation

The experimental validation of the austenite formation kinetics model developed in this work was carried out using an Adamel Lhomargy DT1000 high-resolution dilatometer. The dimensional variations in the specimen are transmitted via an amorphous silica pushrod. These variations are measured by a linear variable differential transformer (LVDT) in a gas-tight enclosure enabling to test under vacuum or in an inert atmosphere. The heating and cooling devices of this dilatometer were also used to perform all the heat treatments. The DT1000 dilatometer is equipped with a radiation furnace for heating. The energy radiated by two tungsten filament lamps is focused on a cylindrical specimen of 2 mm in diameter and 12 mm in length by means of a bi-elliptical reflector. The temperature is measured with a 0.1 mm diameter chromel-alumel (type K) thermocouple spot welded to the specimen. Cooling is

carried out by blowing a jet of helium gas directly onto the specimen surface. The helium flow rate during cooling is controlled by a proportional servovalve. The high efficiency of heat transmission and the very low thermal inertia of the system ensure that the heating and cooling rates ranging from 0.003 Ks^{-1} to 200 Ks^{-1} remain constant.

TABLE III. Temperatures in K of Heating Interruption by Quenching

Morphology of Pearlite	Heating Rate (Ks^{-1})	T_a-5K	T_a	T_b	T_c	T_d	T_e	T_e+10K
	0.05	999	1004	1005	1010	1016	1022	1032
M1	0.5	1005	1010	1011	1018	1026	1031	1041
	5	1014	1019	1023	1026	1041	1050	1060
	0.05	998	1003	1004	1009	1014	1017	1027
M2	0.5	999	1004	1006	1012	1019	1020	1030
	5	1002	1007	1012	1019	1026	1039	1049
	0.05	996	1001	1003	1009	1014	1019	1029
M3	0.5	998	1003	1006	1011	1017	1020	1030
	5	1001	1006	1008	1011	1019	1031	1041

To analyze the progress of pearlite-to-austenite transformation, interrupted heating experiments were carried out by quenching. Dilatometric specimens with three different scales of lamellar pearlite were heated at three different constant rates (0.05, 0.5 and 5 Ks^{-1}). Each test was repeated three times. Heating dilatometric curves were analyzed to determine the start temperature (Ac_1) and the end temperature (Ac_3) of pearlite-to-austenite transformation and then several quench-out temperatures were selected in order to investigate the progress of the transformation. Ac_1 corresponds to the temperature on dilatometric curves

at which expansion deviates from a linear relation during heating and the sample starts to shrink due to austenite formation, whereas Ac_3 is the temperature at which expansion begins again to depend linearly on temperature once sample is fully austenitized; Figure 5 shows the selected quench-out temperatures on a dilatometric curve. They were defined as follows: T_a-5 K being $T_a=Ac_1$; T_b, T_c, and T_d, are the temperatures at the maximum, inflexion point and minimum, respectively, of the heating dilatometric curve; $T_e=Ac_3$ and T_e+10 K. All these temperatures, at which heating was interrupted by quenching for each morphology of pearlite and for each heating rate, are listed in Table III. The temperature reading presented in Table III correspond to the average values of three individual tests.

Austenite, which is formed inside pearlite, transforms to martensite during quenching. Thus, the progress of pearlite-to-austenite transformation is determined throughout the evolution of the volume fraction of martensite. Specimens from interrupted heating experiments were polished in the usual way for metallographic examination. Le Pera's reagent[17] was used to reveal martensite formed during quenching. The quantitative measurement of martensite volume fraction was determined by point counting.[14]

Figure 6 shows microscopic evidences of how the pearlite-to-austenite reaction occurs for the three morphologies of pearlite and for a heating rate of 5 Ks^{-1} throughout micrographs from interrupted heating samples at the start, intermediate and finish stages of the reaustenitization process. Le Pera's reagent[17] reveals pearlite as a darker phase in the microstructure, whereas martensite formed during quenching appears as lighter regions in the micrographs. Microstructures in Figs. 6(a), (d) and (g) are formed mainly of pearlite and some grains of martensite. At these quench-out temperatures, the pearlite-to-austenite transformation starts, and those temperatures are considered the transformation start temperature, T_s, of the three different morphologies of pearlite. Figures 6(b), (e) and (h) show an intermediate stage of the reaction. Finally, Figs. 6(c), (f) and (i) represent microstructures

formed mainly of martensite. At this stage, the transformation pearlite-to-austenite has reached completion and those quench-out temperatures are considered the transformation finish temperature, T_f, of the three different morphologies of pearlite.

III. RESULTS AND DISCUSSION

A. Modeling of continuously heated austenite formation kinetics

Nucleation and growth processes under isothermal condition can be described in general using the Avrami's equation[18]:

$$x = 1 - exp\left(-Kt^n\right) \qquad [5]$$

where x represents the formed austenite volume fraction, K is a constant for a given temperature, t is the time and n is a constant characterizing the kinetics. Roosz et al.[8] obtained a value of n=4 from their measured data under isothermal condition. According to Christian[19], with a spherical configuration, a value of n=4 means that the nucleation rate ($\dot{N}$) and the growth rate (G) are constant in time. This gives a transformed volume fraction of:

$$x = 1 - exp\left(-\frac{\pi}{3}\dot{N}\,G^3 t^4\right) \qquad [6]$$

Roosz et al.[8] proposed the following temperature and structure dependence of nucleation and growth rates as a function of the reciprocal value of overheating ($\Delta T = T\text{-}Ac_1$) since their experimental $\dot{N}$ and G values vs ΔT were able to approximate by a straight line,

$$\dot{N} = f_N \exp\left(\frac{-Q_N}{k\Delta T}\right) \qquad [7]$$

$$G = f_G \exp\left(\frac{-Q_G}{k\Delta T}\right) \qquad [8]$$

where Q_N and Q_G are the activation energies of nucleation and growth, respectively, k is Boltzmann's constant, and f_N and f_G are the functions representing the influence of the structure and heating rate on the nucleation and growth rates, respectively. The activation energies of nucleation and growth, Q_N and Q_G, were determined experimentally by Roosz et al.[8] in a eutectoid steel ($Q_N = 3.5\times10^{-22}$ J/atom and $Q_G = 4.1\times10^{-22}$ J/atom).

Figure 7 shows the three different ferrite/cementite interface sites for austenite nucleation in fully pearlitic steels: A) the interface of ferrite and cementite platelets, B) the surfaces of the pearlite colony, and C) the triple points of the pearlite colony intersections. Several authors[7-9] reported that the nucleation of austenite inside pearlite takes place preferentially at the points of intersection of cementite with the edges of the pearlite colony (type C).

Approximating the pearlite colony as a truncated octahedron, the number of nucleation sites per unit volume (type C) is calculated as follows[16]:

$$N_C = \frac{\left(\frac{36}{3} \quad \frac{a^P}{\sigma_o}\right)}{8\sqrt{2}\left(a^P\right)^3} = \frac{36a^P}{24\sqrt{2}\left(a^P\right)^3\sigma_o} \approx \frac{1}{(a^P)^2\sigma_\circ} \qquad [9]$$

where a^P is the edge length of the pearlite colony and σ_o is the interlamellar spacing.

Bearing in mind that the rate of nucleation increases as the pearlite interlamellar spacing decreases and the edge length of the pearlite colony increases[20], and considering that the heating rate ($\dot{T}$) might influence on the nucleation rate, the function f_N in equation [7] is assumed to have the following general form:

$$f_N = K_N \frac{\left(a^P\right)^n}{\sigma_o^m}\left(\dot{T}\right)^p (N_C)^{r\dot{T}} \qquad [10]$$

where K_N, n, m, p and r are empirical parameters. These parameters were adjusted by multidimensional least squares in order to obtain good fit between theory and the experimental austenite volume fraction curves.

Different cases of structure and heating rate dependence for n, m, p and r were investigated and it was found out that the measured values of austenite volume fraction as a function of temperature can be best described with n=6, m=1, $p=\frac{1}{2}$ and $r=\frac{1}{3}$.

Austenite nuclei in pearlite grow when carbon atoms are transported by diffusion to the ferrite/austenite boundary from the austenite/cementite boundary through the austenite and from the ferrite/cementite boundary through the ferrite, resulting in a transformation of the ferrite lattice to an austenite lattice.[10] As in the case of the reverse transformation (austenite-to-pearlite transformation)[21-23], the growth rate of austenite is believed to be controlled by

either volume diffusion of carbon or by boundary diffusion of substitutional alloying elements such as manganese.[3-24]

If the growth rate of austenite is controlled by the bulk diffusion of atoms in austenite ahead of the interface, the diffusion of carbon may play a more important role than that of substitutional alloying elements. Diffusivity of manganese in austenite is far smaller than that of carbon. As a result, the manganese may not diffuse a long distance during the reaction. However, as described by Porter[25], when temperature decreases, boundary diffusion of substitutional alloying elements is the dominant mechanism in the diffusion process. In that case, the partitioning of manganese is substantial during the growth of austenite and boundary diffusion of manganese may control the growth rate of pearlite.

The function f_G in equation [8] representing the structure dependence on the growth rate can be expressed as follows:

$$f_G = K_G \frac{1}{\sigma_\circ^i} \qquad [11]$$

where K_G is a empirical constant, i=1 if the growth rate of austenite is controlled by volume diffusion of carbon and i=2 if the growth rate of austenite is controlled by boundary diffusion of substitutional alloying elements[8].

Substituting equations [10] and [11] in equations [7] and [8], respectively:

$$\dot{N} = 1.5\times10^{12} \frac{\left(a^P\right)^6}{\sigma_o} \left(\dot{T}\right)^{\frac{1}{2}} (N_C)^{\frac{\dot{T}}{3}} \exp\left(\frac{-25.38}{\Delta T}\right) \quad \text{in } \left(1/\text{mm}^3\text{s}\right) \qquad [12]$$

$$G = 1\times10^{-10} \frac{1}{\sigma_\circ^i} \exp\left(\frac{-29.7}{\Delta T}\right) \quad \text{in } (\text{mm/s}) \qquad [13]$$

K_N and K_G empirical constants were adjusted from the experimental austenite volume fraction results.

The difficulties in treating non-isothermal reactions are meanly due to the independent variations of growth and nucleation rates with temperature, described in equations [12] and [13]. The problem is only undertaken when the rate of transformation depends exclusively on the state of the assembly and not on the thermal path by which the state is reached.[19] Reactions of this type are called isokinetic. Avrami defined an isokinetic reaction by the condition that the nucleation and growth rates are proportional to each other (i.e. they have the same temperature variation). This leads to the concept of additivity and Scheil's rule.[26]

Since Avrami's condition for an isokinetic reaction is not satisfied for the current experimental study, a general equation to describe the non-isothermal overall pearlite-to-austenite transformation in pearlitic steel was derived integrating the Avrami's equation over the whole temperature range where the transformation takes place.[27] In this sense, we have taken logarithms in equation [6] and then it was differentiated,

$$d\left(ln\frac{1}{1-x}\right)=\frac{dx}{1-x}=\frac{4\pi}{3}\dot{N}\,G^3t^3dt \qquad [14]$$

If we consider a constant rate for the heating condition, time can be expressed as follows:

$$dt=\frac{dT}{\dot{T}} \qquad t=\frac{\Delta T}{\dot{T}} \qquad [15]$$

and substituting into equation [14]:

$$\frac{dx}{1-x} = \frac{4\pi}{3}\dot{N}\,G^3\,\frac{\Delta T^3}{\left(\dot{T}\right)^4}\,dT \qquad [16]$$

Integrating in equation [16] in $[0, x]$ and $[Ac_1, T]$ intervals on the left and on the right sides, respectively, it can be concluded that:

$$x = 1 - exp\left(- \int_{Ac_1}^{T} \frac{4\pi}{3\left(\dot{T}\right)^4}\dot{N}\,G^3 \Delta T^3 dT \right) \qquad [17]$$

where $\dot{N}$ and G are given by equations [12] and [13].

Recent authors' work[28] showed that the degree of partition of manganese is the same in the three different initial microstructures since the decomposition of austenite into pearlite is controlled by the diffusion of carbon in the austenite in this steel for the three temperatures studied. Therefore, it has been assumed that at a heating rate higher than 0.5 Ks^{-1} the growth rate of austenite would be mainly controlled by the volume diffusion of carbon in austenite, due to the fact that the transformation would take place mostly at higher temperatures. Consequently, an *i* value of 1 is considered in equation [13] for that case. On the contrary, at heating rates lower than or equal to 0.5 Ks^{-1} the growth rate of austenite has been assumed to be controlled by boundary diffusion of manganese and an *i* value of 2 is considered in equation [13] for that case. The eutectoid temperature Ac_1 of the steel was obtained using Andrews' formula.[29]

B. Experimental validation of the model

Figure 8 shows the experimental and calculated austenite formation kinetics plotted as a function of temperature for three different morphologies of pearlite and three different constant rates (0.05, 0.5 and 5 Ks^{-1}). R^2 is the square correlation factor of the experimental and calculated volume fraction of austenite formed at different temperatures. This parameter quantifies the accuracy of the model. The figure suggests that austenite transformation starts later and appears to be slower the coarser the initial pearlite microstructure and the higher the heating rate. Experimental results for the austenite volume fraction are in good agreement with the predicted values from the model proposed in this work. The accuracy of this model is in the three cases higher than 90% which can be considered excellent for a kinetics model bearing in mind the experimental difficulties for its validation.

Comparison between experimental and calculated results of start (T_s) and (T_f) finish temperatures of pearlite-to-austenite transformation is shown in Figures 9.a and 9.b, respectively. T_s temperature is considered to be the temperature at which a volume fraction of austenite of 0.01 is formed during continuous heating. Moreover, T_f temperature has been defined as the temperature at which a volume fraction of austenite of 0.99 is present in the microstructure. Points lying on the line of unit slope show perfect agreement between experimental and calculated values. The accuracy of the calculations is quantified by R^2.

Calculation of T_s temperatures predicts well the experimental values for 0.05 and 0.5 Ks^{-1} heating rates. However, at the fastest heating (5 Ks^{-1}), the model underestimates (in no more than 5 K) the start temperature for austenite formation. Figure 9.a suggests that at low heating rates close to equilibrium, the calculated results match perfectly those obtained experimentally. The higher the heating rate, the bigger difference between predicted and experimental T_s temperatures. Likewise, Figure 9.b shows an excellent agreement between experimental and predicted values of T_f temperatures (R^2 of 0.95). Small differences between

both values suggest that the model slightly overestimates the effect of the kinetics on the T_f temperatures at the lowest heating rate (0.05 Ks^{-1}) (see also Figure 8).

Variation of experimental T_s and T_f temperatures as a function of heating rate is shown in Figure 10 for the three different morphologies of pearlite. These results suggest that both T_s and T_f temperatures increase with heating rate. The beginning of the pearlite-to-austenite transformation is delayed about 20 K as heating rate is increased from 0.05 to 5 Ks^{-1} for M1 sample, whereas the transformation reaches its completion at a temperature 40 K higher as heating rate is increased from 0.05 to 5 Ks^{-1} for the same scale of pearlite. On the other hand, Figure 10 also shows that the influence of heating rate on both temperatures is less significant the finer the initial pearlite microstructure. Nevertheless, it can be concluded that T_f temperatures are more sensitive to the heating rate than T_s temperatures for the three different scales of lamellar pearlite. It is therefore important to include the scale of initial pearlite and the heating rate as fundamental variables in the austenitization process during the heat treatment of steels.

IV. CONCLUSIONS

1) Since conditions to apply Scheil's rule are rarely satisfied, a mathematical model applying the Avrami's equation has been used to reproduce the kinetics of the pearlite-to-austenite transformation in a eutectoid steel during continuous heating. The model proposes two functions, f_N and f_G, which represent the dependence of nucleation and growth rates, respectively, on the structure and heating rate.
2) The influence of structure parameters, such as interlamellar spacing and edge length of pearlite colonies, and heating rate on the transformation kinetics has been experimentally studied. It has been found that austenite transformation starts later and appears to be

slower the coarser the initial pearlite microstructure and the higher the heating rate. Furthermore, both start and finish temperatures slightly increase as heating rate does, but finish temperatures of the pearlite-to-austenite transformation are more sensitive to the heating rate than start temperatures. However, the influence of heating rate on both temperatures is less significant the finer the initial pearlite microstructure.

3) Experimental results for the austenite volume fraction and critical temperatures of pearlite-to-austenite transformation are in good agreement (accuracy higher than 90% in square correlation factor) with the predicted values from the model proposed in this work.

ACKNOWLEDGEMENTS

The authors acknowledge financial support from Consejería de Educación y Cultura de la Comunidad Autónoma de Madrid (CAM 07N/0065/1998).

REFERENCES

1. H.K.D.H. Bhadeshia, and L.E. Svensson: *Mathematical Modelling of Weld Phenomena*, The Institute of Materials, London, 1993, p. 109.
2. C.I. García, and A.J. DeArdo: *Met. Trans. A.* 1981, vol. 12A, pp. 521-530.
3. G.R. Speich, V.A. Demarest and R.L. Miller: *Met. Trans. A.* 1981, vol. 12A, pp. 1419-1428.
4. M.M. Souza, J.R.C. Guimaraes and K.K. Chawla: *Met. Trans. A.* 1982, vol. 13A, pp. 575-579.
5. Xue-Ling Cai, A.J. Garrat-Reed and W.S. Owen: *Met. Trans. A.* 1985, vol. 16A, pp. 543-557.
6. C. García de Andrés, F.G. Caballero and C. Capdevila: *Scripta Mater.*, 1998, vol. 38, pp. 1835-1842.
7. G.R. Speich and A. Szirmae: *Trans. TMS-AIME*, 1969, vol. 245, pp. 1063-1074.
8. A. Roosz, Z. Gacsi and E. G. Fuchs: *Acta Metall.*, 1983, vol. 31, pp. 509-517.
9. R.R. Judd and H. W. Paxton: *Trans. TMS-AIME*, 1968, vol. 242, pp. 206-215.
10. M. Hillert, K. Nilsson and L.E. Torndahl: *J. Iron and Steel Inst.*, 1971, vol. 209, pp. 49-66.
11. D.P. Datta, and A.M. Gokhale: *Metall. Trans. A.* 1981, vol. 12A, pp. 443-450.
12. E. Navara and R. Harrysson: *Scripta Metall.*, 1984, vol. 18, pp. 605-610.
13. S.F. Dirnfeld, B.M. Korevaar and F. Van't Spijker: *Metall. Trans.*, 1974, vol. 5, pp. 1437-1444.
14. E.E. Underwood: *Quantitative Stereology*, Addison-Wesley Publishing Co., Reading, 1970, pp. 73-75.

15. S.A. Saltykov: *Stereometric Metallography*, 2nd ed., Metallurgizdat, Moscow, 1958, pp. 267-701.
16. R.T. De Hoff, and F.H. Rhines: *Quantitative Stereology*, McGraw-Hill, New York, 1968, p. 93.
17. F.S. Le Pera: *J. of Metals*, 1980, vol. 32, pp. 38-39.
18. M. Avrami: *J. Chem. Phys.*, 1940, vol. 8, pp. 212-.
19. J.W. Christian: *The Theory of Transformations in Metals and Alloys*, Pergamon Press, Oxford, 1975, p. 19.
20. G.A. Roberts and R.F. Mehl, *Trans. ASM*, 1943, vol. 31, pp. 613-650.
21. C. Zener: *Trans. AIME*, 1946, vol. 167, pp. 550-595.
22. M. Hillert: *Jernkont. Ann*., 1957, vol. 141, pp. 757-764.
23. M. Hillert: *The Mechanism of Phase Transformation in Crystalline Solids*, Institute of Metals, London, 1969, p. 231.
24. E. Navara, B. Bengtsson, and K.E. Easterling: *Materials Science and Technology*, 1986, vol. 2, pp. 1196-1201.
25. D.A. Porter and K.E. Easterling: *Phase Transformations in Metals and Alloy*, 2nd ed., Chapman and Hall, London, 1992, p. 101.
26. R. G. Kamat, E.B. Hawbolt, L.C. Brown, and J.K. Brimacombe: *Metall. Trans. A.*, 1992, vol. 23A, pp. 2469-2482.
27. C. García de Andrés, F.G. Caballero, C. Capdevila and H.K.D.H. Bhadeshia: *Scripta Mater.*, 1998, vol. 39, pp. 791-796.
28. F.G. Caballero, C. Capdevila and C. García de Andrés: *Scripta Mater.*, 2000, vol. 42, pp. 537-542.
29. K.W. Andrews: *JISI*, 1965, vol. 203, pp. 721-727.

Fig. 1—Optical micrographs of the three different morphologies of pearlite considered in this study (Table I): (a) M1; (b) M2; (c) M3.

Fig. 2—Electron micrographs of the three different morphologies of pearlite considered in this study (Table I): (a) M1 (SEM); (b) M2 (SEM); (c) M3 (TEM).

Fig. 3—(a) Scheme and (b) Typical example of scanning electron micrograph used to quantify the area per unit volume of the pearlite colonies interface, S_V^{PP}.

Fig. 4—Truncated octahedron.

Fig. 5—Temperatures selected from heating dilatometric curves to investigate the progress of pearlite-to-austenite transformation.

Fig. 6—Optical micrographs corresponding to the start (T_s), intermediate (T_i) and finish (T_f) temperatures of the reaustenitization process. (a) T_s, M1; (b) T_i, M1; (c) T_f, M1; (d) T_s, M2; (e) T_i, M2; (f) T_f, M2; (g) T_s, M3; (h) T_i, M3; (i) T_f, M3; Heating rate of 5 K/s.

Fig. 7—Scheme of the ferrite/cementite interface sites for austenite nucleation in fully pearlitic steel.

Fig. 8—Experimental and calculated kinetics results for the formation of austenite inside pearlite under continuous heating conditions in eutectoid steel.

Fig. 9—Comparison of experimental and calculated (a) start (T_s) and (b) finish (T_f) temperatures of pearlite-to-austenite transformation in a eutectoid steel.

Fig. 10—Experimental variation in (a) start (T_s) and (b) finish (T_f) temperatures of pearlite-to-austenite transformation as function of heating rate.

Fig. 1—Optical micrographs of the three different morphologies of pearlite considered in this study (Table I): (a) M1; (b) M2; (c) M3.

Fig. 2—Electron micrographs of the three different morphologies of pearlite considered in this study (Table I): (a) M1 (SEM); (b) M2 (SEM); (c) M3 (TEM).

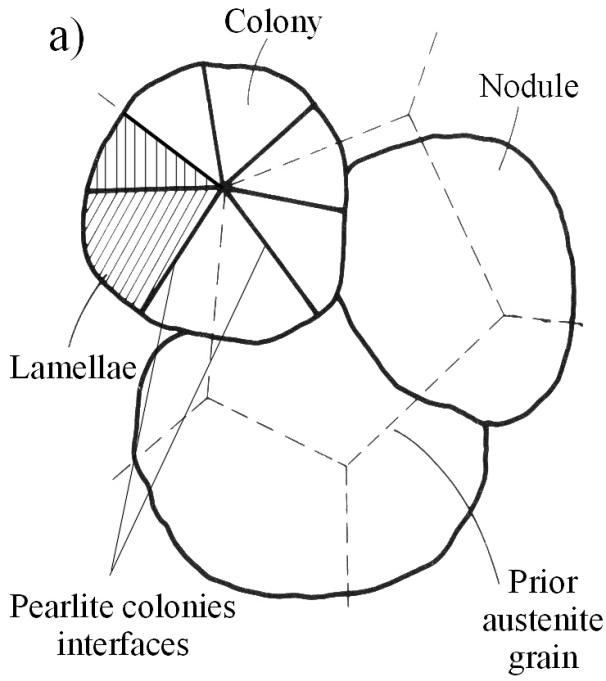

Fig. 3—(a) Scheme and (b) Typical example of scanning electron micrograph used to quantify the area per unit volume of the pearlite colonies interface, S_V^{PP}.

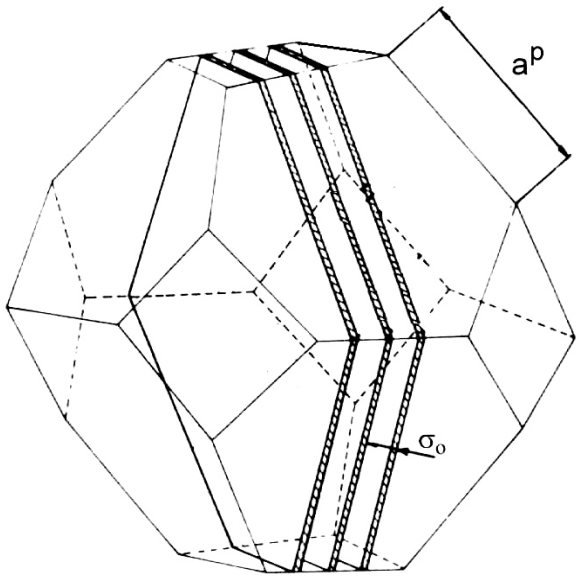

Fig. 4—Truncated octahedron.

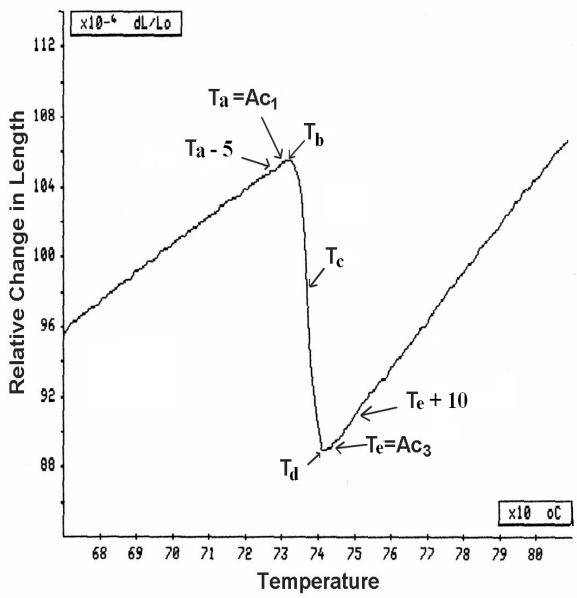

Fig. 5—Temperatures selected from heating dilatometric curves to investigate the progress of pearlite-to-austenite transformation.

Fig. 6—Optical micrographs corresponding to the start (T_s), intermediate (T_i) and finish (T_f) temperatures of the reaustenitization process. (a) T_s, M1; (b) T_i, M1; (c) T_f, M1; (d) T_s, M2; (e) T_i, M2; (f) T_f, M2; (g) T_s, M3; (h) T_i, M3; (i) T_f, M3; Heating rate of 5 Ks^{-1}

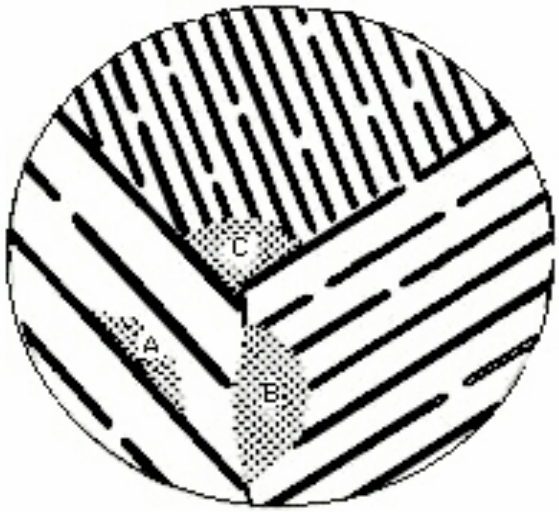

Fig. 7—Scheme of the ferrite/cementite interface sites for austenite nucleation in fully pearlitic steel.

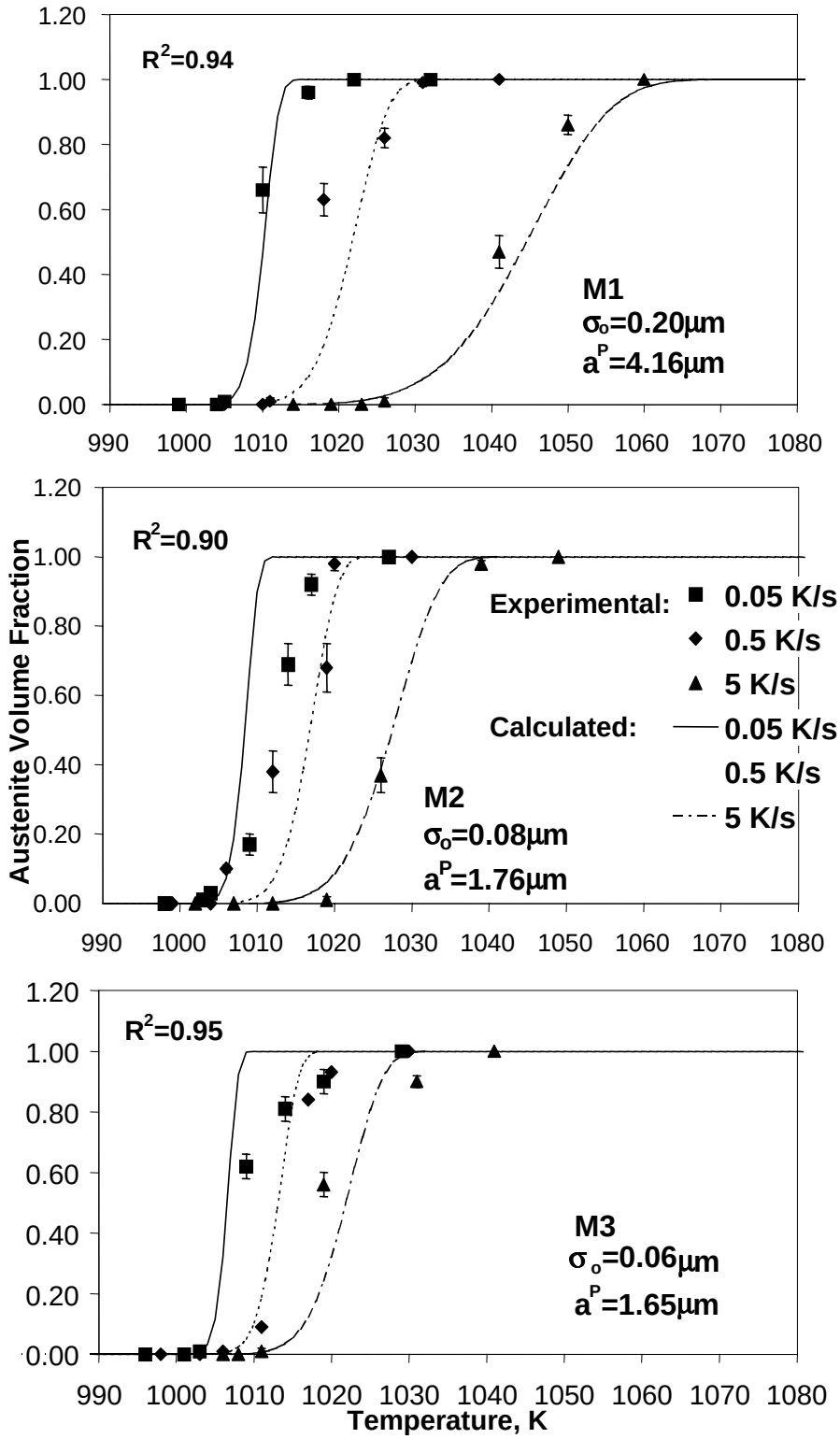

Fig. 8—Experimental and calculated kinetics results for the formation of austenite inside pearlite under continuous heating conditions in eutectoid steel.

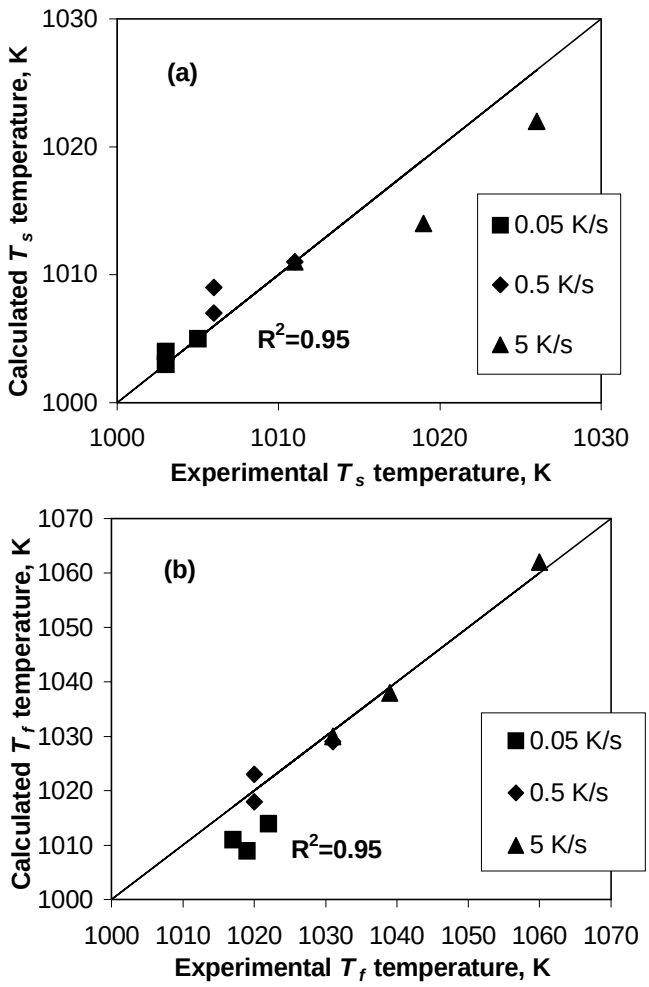

Fig. 9—Comparison of experimental and calculated (a) start (T_s) and (b) finish (T_f) temperatures of pearlite-to-austenite transformation in a eutectoid steel.

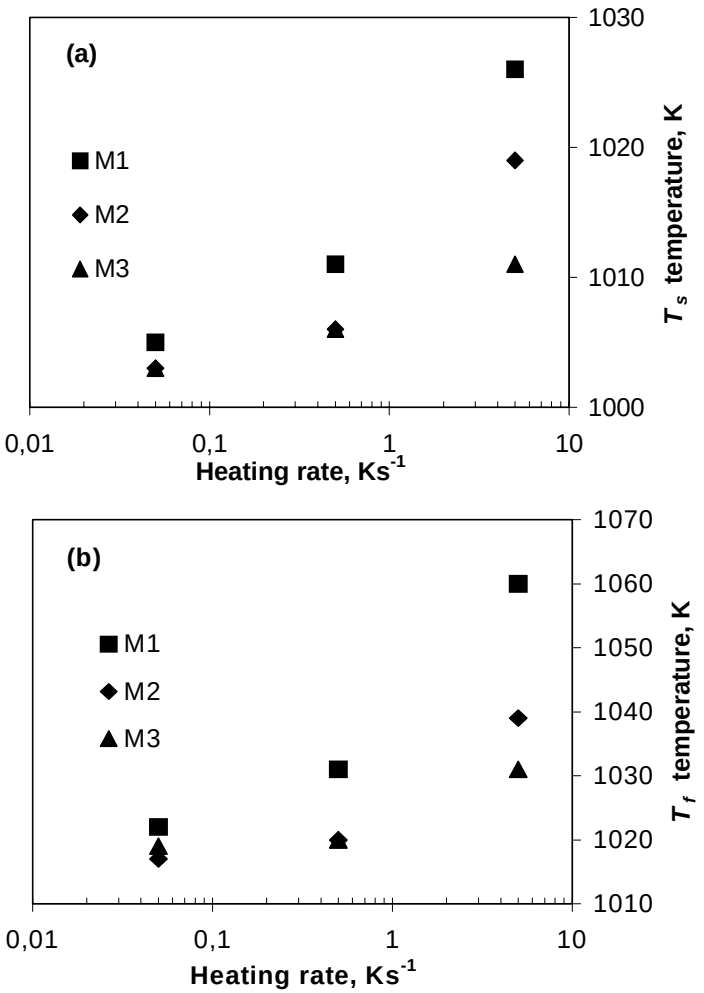

Fig. 10—Experimental variation in (a) start (T_s) and (b) finish (T_f) temperatures of pearlite-to-austenite transformation as function of heating rate.